THE ASTROPHYSICAL JOURNAL, 383:95–103, 1991 December 10

EXPECTATIONS FOR X-RAY CLUSTER OBSERVATIONS BY THE *ROSAT* SATELLITE

A. E. EVRARD
Department of Physics, 1049 Randall Lab, University of Michigan, Ann Arbor, MI 48103
AND
J. P. HENRY[1]
Max-Planck-Institut für Extraterrestrische Physik, 8046 Garching bei München, Germany
Received 1991 March 21; accepted 1991 June 19

ABSTRACT

We present predictions for characteristics of the X-ray cluster population expected to be observed by the *ROSAT* satellite. The theoretical modeling requires an assumed fluctuation spectrum and relations describing the behavior of cluster X-ray luminosity and core radius with cluster binding mass and redshift.

The most "natural" model, which assumes self-similar scaling $L_x \propto M^{4/3}$ in a cold dark matter (CDM) universe, fails to reproduce the shape of the local X-ray cluster luminosity function. For CDM to be successful, the bolometric X-ray luminosity L_x must scale with binding mass M as $L_x \propto M^3$, perhaps indicative of a strong dependence of intracluster gas fraction with mass. An alternative model motivated by recent evidence for more large-scale power, uses an $n = -2$ initial fluctuation spectrum and fits local cluster abundances with an intermediate scaling $L_x \propto M^{11/6}$. This scaling law may imply a fixed minimum entropy for the gas in the cores of rich clusters, perhaps a signature of activity from an earlier galaxy formation era.

For the north ecliptic pole region of the *ROSAT* all-sky survey, which will cover a 10° radius field to a limiting flux of roughly 9×10^{-14} ergs s^{-1} cm^{-2}, the successful models predict $\sim$330 cluster X-ray sources visible above the flux limit if a square detect cell of side 4.8 is employed. The clusters would have a median redshift of 0.2, and 10% of them should have $z > 0.4$ but essentially none should be seen at $z > 1$. Roughly 2500 clusters are expected with this detect geometry in the all-sky survey above the limiting flux of 7×10^{-13} ergs s^{-1} cm^{-2}. Cluster sources would be expected to contribute $\sim$10% of the observed soft X-ray background. The sensitivity of cluster detectability to treatment of the core emission and detect cell geometry is the principal source of uncertainty in these predictions.

Subject headings: dark matter — galaxies: clustering — galaxies: X-rays

1. INTRODUCTION

The *ROSAT* satellite (Truemper 1984) successfully launched on 1990 June 1 has completed the first all-sky imaging survey at X-ray wavelengths. The data obtained will greatly improve our uderstanding of the structure and evolution of cosmic X-ray sources. Clusters of galaxies represent a significant and interesting class of X-ray emitters whose structure and evolution to even modest redshifts $z \simeq 0.2$ is presently poorly understood (see the review by Sarazin 1986). The *ROSAT* survey, particularly the deep regions at the ecliptic poles, represents a significant improvement in sensitivity and coverage over previous surveys such as the *Einstein* EMSS (Gioia et al. 1990b) and the *HEAO 1* survey (McKee et al. 1980). It is expected that this data base will provide new understanding of the evolution of cluster X-ray emission, perhaps even to redshifts $z \simeq 1$.

In this paper, we employ empirically fit models to address expectations for the cluster population in the context of the *ROSAT* survey. The theoretical machinery requires a specific cosmological model as well as assumptions regarding the dynamical evolution of the intracluster medium (ICM) with cluster binding mass and redshift. Working within the gravitational instability picture of large-scale structure formation (Peebles 1980), we explore both the popular cold dark matter (CDM) spectrum (Peebles 1982; Blumenthal et al. 1984; Davis et al. 1985) as well as a scale-free spectrum with spectral index $n = -2$. The latter model provides more power on large scales than CDM—a characteristic which appears warranted by recent observations of galaxy clustering (Broadhurst et al. 1990; Maddox et al. 1990; Efstathiou et al. 1990) as well as the cluster X-ray temperature distribution (Henry & Arnaud 1991). We assume a critical density $\Omega = 1$, the majority of which is dark matter, and Hubble constant $H_0 = 50$ km s^{-1} Mpc^{-1} throughout. A similar study incorporating detailed instrument response but assuming a nonevolving cluster population has been performed by Cruddace, Hasinger, & Hartner (1991).

The nature of the collisionless, dark matter distribution in the nonlinear regime is fairly well understood from N-body experiments (e.g., Efstathiou et al. 1988). These experiments indicate that the abundance distribution of dark matter potential wells can be inferred directly from the initial fluctuation spectrum using the Press-Schechter formula (Press & Schechter 1974; Bond et al. 1991). To predict the X-ray emission expected from baryons collapsed into these dark matter wells, we require additional information on the dynamics and thermodynamics of the baryonic component which comprises the cluster ICM. If shock heating from gravitational collapse is the dominant mechanism driving the ICM evolution and if a constant fraction of the baryonic content of the universe ends up as intracluster gas, then the self-similar model detailed by Kaiser (1986) is the natural expectation. We find below that this model, coupled to the expected abundance of halos in the CDM cosmology, is ruled out by present data on the local

[1] On leave from Institute for Astrophysics, University of Hawaii.

X-ray cluster luminosity function. We then explore two alternative models—one based on CDM, the other on an $n = -2$ spectrum—which are designed to match the abundances of the local cluster population. For these models, we investigate the implications for the *ROSAT* survey in terms of a cluster log N–log S and the associated counts of clusters expected in the all-sky survey, particularly the north ecliptic pole (NEP) region.

The two successful models make nearly identical predictions for the counts of clusters expected to be seen by *ROSAT*. However, the models have distinguishing characteristics which are highlighted, namely, the expected counts as a function of cluster temperature, the T-L relation, and the spectral shape of the X-ray background produced by cluster sources.

Clusters are extended sources with typical angular core scales of $\sim 1'$. Detect algorithms optimized for point sources may miss much of the extended cluster emission, leading to substantial incompleteness and undercounting of the true cluster log N–log S. As recently stressed by Pesce et al. (1990), the degree of incompleteness will depend on the behavior of the cluster core emission. Smaller core radius systems will appear more pointlike and be more easily detected than systems whose core radii are comparable to or larger than the detect cell size. The dominant controlling factors in cluster count predictions are thus the behavior of the cluster core emission with mass and epoch and the details of the detect algorithm used to locate peaks in photon maps.

In the following section, we introduce the theoretical models and fit to the local luminosity function data. Section 3 presents expectations for the *ROSAT* survey in terms of a cluster log N–log S and counts in the deep north ecliptic pole region. A discussion section follows which examines other observable predictions of the models and associated uncertainties. A brief summary is provided in § 5.

2. MODELING THE LOCAL CLUSTER POPULATION

The problem of describing the evolution of the X-ray cluster population in a universe dominated by collisionless dark matter can be split into two logically distinct parts—one to deal with the evolution of the dark matter halo population, the other to deal with the dynamics of the baryonic component within the dark matter potential wells. Such an approach was first applied to X-ray clusters by Perrenod (1980) and has more recently been used in attempts to model the galaxy distribution (Evrard 1989; Cole 1991; White & Frenk 1991).

The Press-Schechter formula (Press & Schechter 1974), recently rederived in a more rigorous form by Bond et al. (1991), provides $n(M, z)$, the number density of collapsed halos as a function of mass M at redshift z

$$n(M, z)dM = -\sqrt{\frac{2}{\pi}}\frac{\rho_o}{M^2}\frac{d\ln\sigma(M)}{d\ln M} \times \nu_z(M)\exp(-\nu_z^2(M)/2)dM , \quad (1)$$

where $\sigma(M)$ is the present linearly evolved rms level of fluctuations on mass scale M, $\nu_z(M) = 1.68(1+z)/\sigma(M)$ is the normalized perturbation just collapsing at redshift z and ρ_o is the present background density. Here, a "halo" is defined as a mass concentration overdense relative to the background by a factor of 170. This is roughly the density at which structures reach hydrostatic and viral equilibrium after collapse from the general cosmological expansion.

It is instructive to characterize locally the fluctuations as a power law in mass

$$\sigma(M) = \sigma_{15} M^{-\alpha} , \quad (2)$$

where the mass M is in units of $10^{15} M_\odot$. For Gaussian spectra with power spectrum $P(k) \propto k^n$, the exponent α is related to the spectral index n by $\alpha = (n+3)/6$ (Peebles 1980). The number density for this case can be written succinctly as

$$n(M, z)dM = n_*(z)M^{-(2-\alpha)}\exp\{-[M/M_*(z)]^{2\alpha}\}dM , \quad (3)$$

where

$$n_*(z) = 9.3\times 10^{-5}\sigma_{15}^{-1}\alpha(1+z)\mathrm{Mpc}^{-3} , \qquad M_*(z) = [1.19\sigma_{15}^{-1}(1+z)]^{-1/\alpha} . \quad (4)$$

Since rich clusters span only about a decade in mass, the above approximation will be accurate for spectra with modest curvature on cluster mass scales. The CDM spectrum is well described as an $n = -1$ power law on scales near $10^{15} M_\odot$, and we use this approximation in our calculations. Results obtained using the true CDM spectrum show no significant differences. For both the $n = -1$ and $n = -2$ models, we normalize the level of fluctuations at $\sigma_{15} = 0.6$ which is equivalent to a bias parameter of $b = 1.7$.

To this we must now add the evolution of the baryonic intracluster medium. In the self-similar model (Kaiser 1986), one starts with the fact that gravity and an initial scale-free spectrum provide no characteristic scales which might imprint features on cluster density or temperature profiles. It follows that all clusters must appear identical when expressed in some appropriate, dimensionless fashion. These dimensional arguments lead to the cluster temperature T and bolometric luminosity $L_{\rm bol}$ scaling as

$$T(M, z) = T_{15} M^{2/3}(1+z) , \qquad L_{\rm bol}(M, z) = L_{15} M^{4/3}(1+z)^{7/2} \quad (5)$$

where the scaling of the luminosity arises from considering that $L_{\rm bol} \propto M\rho T^{1/2}$, with $\rho \propto (1+z)^3$ and T scaling as above. For all models, we assume the above $T(M, z)$ relation holds with normalization $T_{15} = 5$ keV. These scaling laws are reproduced by three-dimensional hydrodynamic simulations incorporating only gravitational effects. This simple model also does remarkably well in reproducing many aspects of the observed X-ray cluster population and provides a plausible resolution for the long-standing "β-discrepancy" regarding the relative specific energies of the galaxies and gas in clusters (Evrard 1990a, b).

Constructing a luminosity function is achieved by employing the luminosity-mass relation with the Press-Schechter abundance function. For a power-law spectrum, an expression similar to equation (3) is obtained (see Appendix A), with a power-law faint end and exponential bright end. The observed luminosity functions are generally expressed using the flux within the energy band of a specific instrument. The cluster luminosity in some energy band can be written

$$L_E(M, z) = L_{\rm bol}(M, z) f_E[T(M, z)] , \quad (6)$$

where $f_E[T(M, z)]$ is the fraction of the bolometric luminosity falling in the specified energy band for a cluster of temperature T. We use an approximate Gaunt factor of $g(E, kT) = 0.9(E/kT)^{-0.3}$ in our calculations. Results intended for comparison

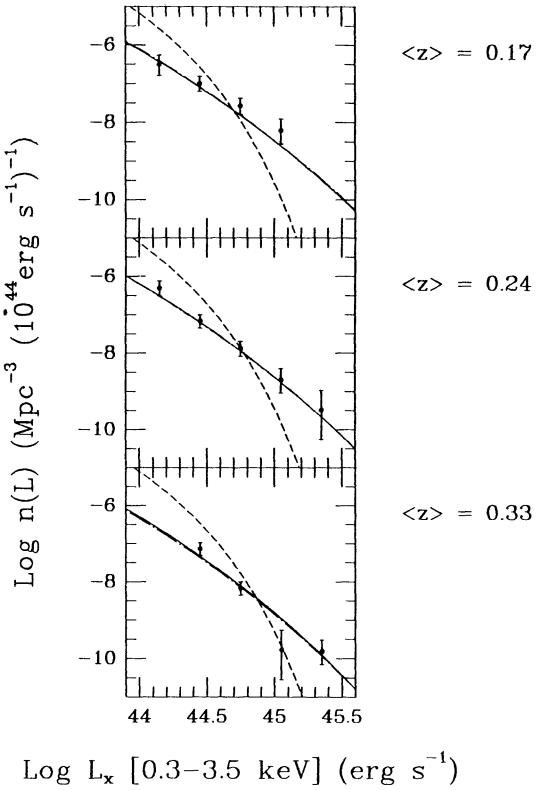

FIG. 1.—The theoretical luminosity functions compared to the observational data in three redshift bins from the *Einstein* EMSS survey (Gioia et al. 1990). The self-similar CDM model (*dashed lines*) does not fit the data. Models CDMP3 (*solid line*) and XCDM (*dot-dashed lines*) are constructed to provide equally good (hence indistinguishable) fits to the EMSS data.

with *Einstein* IPC observations are given in a 0.3–3.5 keV band, while predictions for the *ROSAT* PSPC use a 0.1–2.4 keV energy range. To construct theoretical estimates for the luminosity function within a particular band, we invert equation (6) to calculate the cluster number density at a given band luminosity from equation (3), after first tabulating the band fraction $f_E(T)$.

Figure 1 shows the luminosity function in the 0.3–3.5 keV band predicted at three redshifts using the CDM spectrum and the self-similar relations. These are to be compared with the observational data from the *Einstein* EMSS survey (Gioia et al. 1990a) also shown in the figure. This theoretical model, denoted CDMSS in Table 1, produces a luminosity function which *disagrees in shape* with the observations. The only free parameter in this model is the luminosity-mass relation normalization L_{15}. Varying this parameter only slides the theoretical curve along the horizontal axis and does not affect its shape. The χ^2 for this model is 256 for 12 degrees of freedom, implying the model is ruled out with very high confidence.

TABLE 1

MODEL PARAMETERS

Model	n	L_{15}[a]	p[a]	s[a]	r_o[b]	u[b]	v[b]
CDMSS.....	−1	5.5	4/3	7/2	300	1/3	−1
CDMP3.....	−1	5.5	3	7/2	300	0	0
XCDM.....	−2	7	11/6	11/4	300	−1/6	−1/4

[a] Bolometric luminosity in 10^{44} ergs s^{-1} scaling as $L_{bol} = L_{15} M^p(1+z)^s$.
[b] Core radius in kpc scaling as $r_c = r_o M^u(1+z)^v$.

Although attractive from a theoretical perspective, the simplicity of the self-similar model is undoubtedly its main weakness. The thermal history of the average ICM atom is likely to be much more complex than the model assumes. Observational support for this comes from the observed enrichment of the ICM to roughly half-solar values (Rothenflug & Arnaud 1985), the evidence for central cooling flows (Fabian, Nulsen, & Canizares 1984) and the lack of significant correlations between the X-ray core radius values and other X-ray or optical properties (Abramopolous & Ku 1983; Edge & Stewart 1991).

To accommodate alternatives to the self-similar model, we write a general relation between bolometric luminosity and mass of the form

$$L_{bol}(M, z) = L_{15} M^p (1+z)^s , \quad (7)$$

introducing the parameters p and s to encapsulate all the interesting physics affecting the history of the ICM. The idea is to empirically fit for values of these parameters using data on the luminosity function of clusters to moderate redshifts obtained from the *Einstein* EMSS survey (Gioia et al. 1990a).

Unfortunately, the luminosity function predictions contain an inherent redundancy between the shape of the assumed fluctuation spectrum and the form of the $L(M, z)$ scaling law. This is just another form of the usual problem of trying to distinguish "luminosity" from "number" evolution within a population. This can be seen explicitly for the $z = 0$ luminosity function of a power-law spectrum which has a form (Appendix A)

$$n(L)dL \propto L^{-(p+1-\alpha)/p} \exp\left(-(L/L_*)^{2\alpha/p}\right)dL . \quad (8)$$

Since flux-limited samples access a finite dynamic range in L, unique values of both α and p may be impossible to establish with abundance information alone. This is particularly likely for values of α and p such that $2\alpha/p \ll 1$. In this case, the "knee" in the luminosity function can be stretched out to the point where it becomes indistinguishable from a power law over the observed range of luminosity. The present X-ray cluster luminosity function determinations span about two decades in L (Piccinotti et al. 1982; Johnson et al. 1983; Edge et al. 1990; Gioia et al. 1990a). Most observations are well fitted by a power-law form; inclusion of an exponential bright cutoff provides a slightly better fit to the *EXOSAT* data (Edge et al. 1990).

This redundancy in α and p will allow a family of models to fit the EMSS data. We single out two specific models, CDMP3 and XCDM of Table 1, which produce identically good fits to data shown in Figure 1. Model CDMP3 employs an $n = -1$ spectrum with scaling exponents $p = 3$ and $s = 7/2$. Model XCDM assumes an $n = -2$ spectrum with exponents $p = 11/6$ and $s = 11/4$. The motivation for the $n = -2$ case is that it provides more power on scales larger than $10^{15}\ M_\odot$ than the standard CDM model, a feature for which there is building observational evidence from the APM angular correlation function (Maddox et al. 1990), the clustering of *IRAS* galaxies (Efstathiou et al. 1990) and deep pencil beam surveys (Broadhurst et al. 1990). The shape of the cluster X-ray temperature distribution also favors an index closer to $n = -2$ (Henry & Arnaud 1991).

The physical implications of these models is subject to interpretation. The value of $p = 3$ in model CDMP3 may imply that the ICM fraction is a strong function of cluster binding mass or richness (David et al. 1990). If this were the sole cause

for departure from self-similarity the ICM fraction $f_{\rm ICM}$ would have to vary nearly linearly with cluster mass $f_{\rm ICM} \propto M^{5/6}$. It is not at all clear whether this can be ruled out by present data. For the CDM spectrum, we find acceptable fits to the data for values of p between 2.5 and 3.5 and s between 5/2 and 9/2.

The values of $p = 11/6$ and $s = 11/4$ in model XCDM have an interesting and perhaps appealing interpretation in terms of a minimum central entropy for the cluster gas (see derivation in Appendix B). A minimum entropy for the cluster ICM could be generated from feedback supplied by forming galaxies or quasars during the cluster precollapse phase at a redshift $z \sim 5$. Numerical simulations indicate that generating a core radius in X-rays as large as is observed for Coma, $r_c = 400$ kpc (Hughes 1989), can be achieved by "preheating" the ICM baryons to a temperature of 10^7 K at $z = 7$ (Evrard 1990a). Feedback can effectively set a minimum entropy for the ICM plasma if it heats the gas sufficiently that its cooling time becomes long. The preheating does *not* necessarily imply an isentropic gas distribution within the post-collapse cluster. For the pre-heated Coma model of Evrard (1990a), the central $\sim 10\%$ of the cluster mass behaves adiabatically throughout the collapse, while material infalling later at larger radii arrives farther from equilibrium and experiences an increasing degree of shock heating. The resultant cluster has a nearly isothermal temperature distribution, with an entropy profile consisting of a roughly constant entropy core enveloped by a halo with radially increasing entropy.

3. EXPECTATIONS FOR *ROSAT*

In order to predict the counts of clusters expected to be seen by the *ROSAT* satellite for these models, information on the cluster profile emission and the geometry of the flux measurement must be specified. We assume a standard "β-profile" for the emission, with the surface brightness Σ falling off with angular distance θ as

$$\Sigma(\theta) = \Sigma_o[1 + (\theta/\theta_x)^2]^{-3\beta+1/2} . \quad (9)$$

We take a fixed profile slope $\beta = 2/3$. The angular core radius θ_x depends on the viewing redshift and physical core radius $r_c(M, z)$, which is model-dependent (Table 1). In the self-similar model CDMSS, the core radius scales as $r_c = r_o M^{1/3}(1 + z)^{-1}$. Since model CDMP3 has no unique physical motivation, we assume a constant core radius r_o for the entire population. Model XCDM, the minimum central entropy model, has the core radius scaling weakly with mass and redshift $r_c = r_o M^{-1/6}(1 + z)^{-1/4}$ (Appendix B). We choose a normalization $r_o = 300$ kpc, consistent with the value chosen by Gioia et al. (1990a) in constructing the EMSS luminosity function.

We are now in a position to predict number counts expected to be detected above a given flux level for a specified detect cell geometry. The total cluster flux is the integral of the surface brightness

$$S = \frac{\pi\theta_x^2\Sigma_o}{3(\beta - 1/2)} \quad (10)$$

which is related to the cluster luminosity and redshift by

$$S = \frac{H_o^2}{16\pi c^2} \frac{L}{(1 + z)[(1 + 3)^{1/2} - 1]^2} . \quad (11)$$

We use a square detect cell of 4.'8 on a side. The point response function appropriate to the *ROSAT* telescope + PSPC + survey scan pattern was taken from Hasinger (1985) and is approximately exponential with scale length 1.'6. Integrating the extended cluster emission convolved with the response function over the detect cell area yields the measurable detect cell flux which we express as a fraction f_d of the total cluster flux

$$S_{\rm obs}(\theta_x) = f_d(\theta_x)S . \quad (12)$$

The fraction $f_d(\theta_x)$ is shown in Figure 2*a*. Figure 2*b* shows the fraction as a function of redshift for fixed values of physical core radii equal to 100, 300, and 500 kpc.

The counts of clusters expected above a flux S (the log N–log S relation) for these models is shown in Figure 3. The dark lines show the counts using only the flux expected in the detect cell. The light lines show the expectations if the full cluster flux were observed. The latter can be interpreted as the flux detectable from a cluster population appearing as point sources in a perfect detector. This represents the maximum level of counts

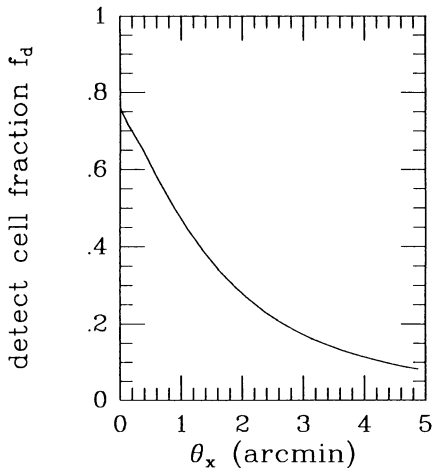

FIG. 2*a*

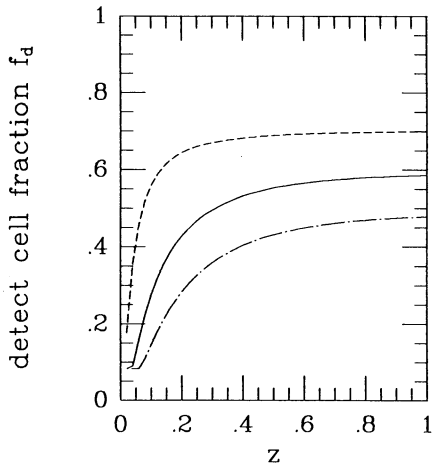

FIG. 2*b*

FIG. 2.—(*a*) The fraction of the total cluster flux measured within a 4.'8 arcmin^2 detect cell incorporating the telescope + instrument + survey response (Hasinger 1985) for a $\beta = 2/3$ profile with angular core radius θ_x. (*b*) The fraction as a function of redshift for clusters with physical core radii equal to 100 (*dashed line*), 300 (*solid line*), and 500 (*dot-dashed line*) kpc.

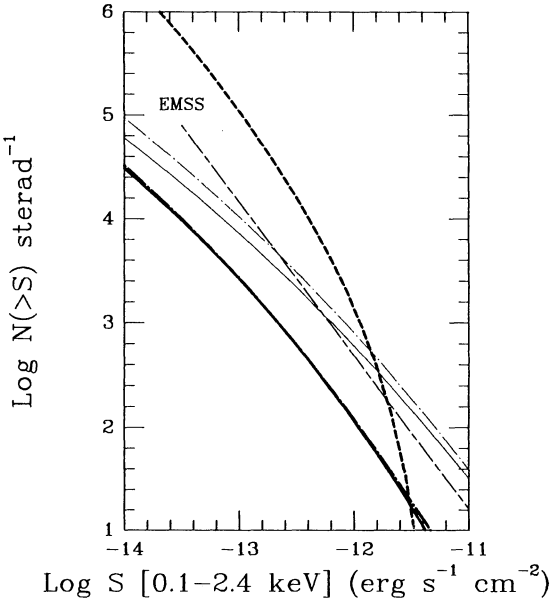

FIG. 3.—The counts of clusters expected as a function of flux in the *ROSAT* band. The heavy lines use the detect cell flux for models CDMSS (*dashed line*), models CDMP3 (*solid line*) and XCDM (*dot-dashed line*). The latter two are nearly indistinguishable. The light lines show the counts expected for models CDMP3 and XCDM if the full cluster flux is used. The straight, dashed line is the log N–log S for *all* sources from the *Einstein* EMSS survey shown for comparison.

expected within each of the models. The straight, dashed line is the EMSS log N–log S for *all* sources (Gioia et al. 1990b) shown for comparative purposes.

The counts from model CDMSS with the detect cell limit on the flux exceed the observed EMSS counts. Counts without the detect cell limited flux are, of course, higher. Again, this is an indication that the model is in serious conflict with local observations. The detect cell–limited counts of models CDMP3 and XCDM fall below the EMSS data. The similar predictions of these models was to be expected since they were both constructed to reproduce the EMSS luminosity function data and their core radii parameterizations are not dramatically different over the mass and redshift ranges probed.

The all-sky survey is expected to have a mean exposure of about 600 s, implying a limiting flux of approximately 7×10^{-13} ergs s^{-1} cm^{-2}. At this limit, models CDMP3 and XCDM predict $\sim$200 clusters per steradian or roughly 2,500 over the entire sky. Since the satellite observes the ecliptic poles on each orbit, the limiting flux at the poles is somewhat deeper, roughly 9×10^{-14} ergs s^{-1} cm^{-2}. This limit applies to the NEP region of the survey, which spans roughly a 10° radius area centered on the pole.

For the NEP region, we expect $\sim$330 clusters above the flux limit using the 4.8 detect cell. The redshift distribution of these sources is shown in Figure 4, which plots both the differential and cumulative counts of clusters with redshifts greater than z. Roughly half the population would have redshifts $z > 0.2$ while 10% would be expected to lie at $z > 0.4$. These models anticipate that *none of these cluster sources should have redshift larger than one.*

Even at the deeper flux level of 1×10^{-14} ergs s^{-1} cm^{-2}, we expect the surface density of clusters with redshifts $z > 1$ to be only 18 per steradian for model CDMP3 and 5.3 per steradian for model XCDM. Barring serendipitous discovery, a large fraction of the sky would have to be surveyed to this depth in order to produce just one cluster with redshift greater than one.

4. DISCUSSION

4.1. *Distinguishing XCDM from CDMP3*

Although models CDMP3 and XCDM predict nearly identical cluster counts for the *ROSAT* survey, there are other X-ray observables potentially capable of discriminating between them. One is the distribution of clusters as a function of X-ray temperature. A recent determination of the temperature abundance function by Henry & Arnaud (1991) based on the flux limited sample of Lahav et al. (1989) favors a spectral index n close to -2. The shape of their abundance function agrees well with the determination by Edge et al. (1990) on essentially the same data set. Henry & Arnaud found a best fit spectral index of $n = -1.7^{+0.65}_{-0.35}$. Formally, their analysis rules out a value of $n = -1$ at the 99.5% confidence level. However, the existence of uncertain systematic effects and the small sample size of 25 clusters currently available complicates interpretation of this analysis.

Figure 5 shows the distribution of cluster temperatures for the NEP region corresponding to the data shown in Figure 4. The cumulative fraction of clusters expected with temperature greater than T is shown for models CDMP3 and XCDM. The clusters in model XCDM span a wider range in T than those of CDMP3—the cumulative distribution is therefore more shallow. Model CDMP3 has $\sim$40% of the NEP clusters with $T > 4$ keV, while model XCDM would expect only $\sim$10% above this temperature.

A related-observable is the correlation between cluster temperature and luminosity. The T-L relations expected within the models are

$$T \propto L_{\rm bol}^{0.22}(1+z)^{0.22}\text{: CDMP3 ,} \qquad T \propto L_{\rm bol}^{0.36}\text{: XCDM .} \tag{13}$$

The *EXOSAT* data compiled by Edge & Stewart (1991) indi-

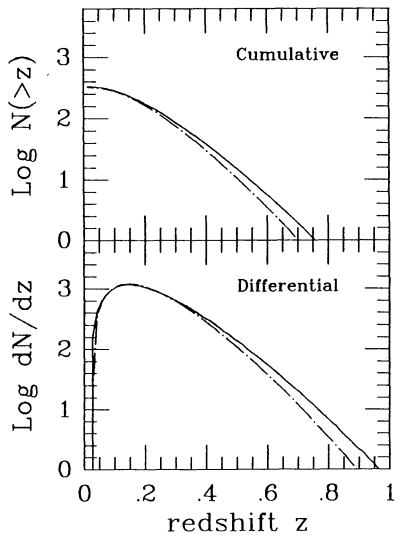

FIG. 4.—The counts of clusters expected in the NEP survey region. The lower panel shows the differential counts; the upper gives the cumulative counts of clusters lying beyond the redshift z. Line styles are the same as in Fig. 3.

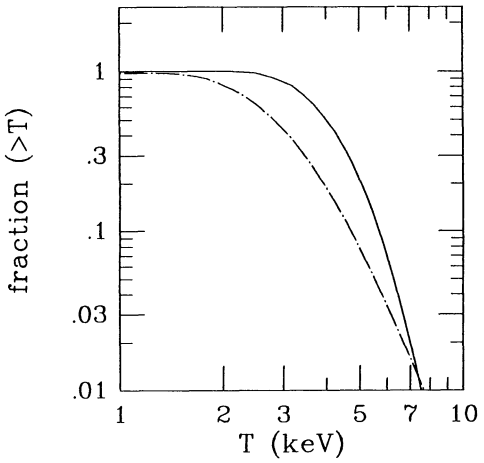

FIG. 5.—The cumulative fraction of clusters with temperature greater than T for the NEP clusters shown in Fig. 4. Model XCDM (*dot-dashed line*) predicts a broader observable temperature range than model CDMP3 (*solid line*).

cate that

$$T \propto L_{\rm bol}^{0.30\pm0.05} : EXOSAT \qquad (14)$$

which unfortunately, straddles midway between the two models. Note that although there is no redshift dependence in the temperature-luminosity relation for model XCDM, the z-dependence in model CDMP3 is so mild that it does not present a realistically useful test.

The validity of any test based on cluster X-ray temperature hinges on the assumption that the ICM temperature scales linearly with the depth of the dark matter potential well $T \propto M^{2/3}(1+z)$. One way this assumption could be violated is if heat input from galaxies is an important factor in determining the gas temperature. This may be more likely true in poorer clusters with shallower potential wells (White 1990). Data from *EXOSAT* on the ratio of gas temperature to galaxy velocity dispersion in clusters provide some evidence for this effect (Edge & Stewart 1991; Evrard 1990b).

Another, more speculative discriminator is the contribution of clusters to the X-ray background (XRB) spectrum. Figure 6 shows the XRB spectrum expected from clusters with redshifts $z > 0.2$. Neutral hydrogen absorption is ignored in computing the incident flux, an approximation valid for column densities lower than $\sim 10^{20}$ cm^{-2}. The *Einstein* IPC observations taken from Wu et al. (1991) are also shown. Except for the lowest energy bin, these observations are in agreement with the Wisconsin results of McCammon et al. (1983). It is clear that, in either model, clusters will produce only $\sim 10\%$ of the observed soft XRB. However, at such soft energies, it is not presently known whether the bulk of the observed photons are galactic or extragalactic in origin (McCammon & Sanders 1990). If thermal emission from 10^6 K gas in the galaxy dominates the flux below ~ 1 keV, then it may be possible that clusters contribute a substantial fraction of the soft, *extragalactic* XRB (Blanchard et al. 1992). Figure 6 indicates that the two models predict fluxes differing by a factor 4 at 0.1 keV. This difference arises from the different mass and temperature ranges being probed in each model, as illustrated in Figure 5. The lower temperature clusters in model XCDM produce the excess of soft photons relative to model CDMP3 seen in Figure 6.

4.2. *Cluster Detectability*

As recently emphasized by Pesce et al. (1990), assumptions regarding the behavior of cluster core emission can significantly affect the visibility of clusters within a fixed detect area and thereby significantly affect count predictions. Pesce et al. point out that central cooling flows act essentially as point sources superposed onto the more extended general cluster emission. Allowing for a range of relative cooling flow contributions (determined from observations), they find the counts expected in the EMSS survey, which employed a 2.4 arcmin^2 detect cell, vary by a factor of ~ 20 between cases with no cooling flow contribution versus cases including the central excess.

Our analysis does not differentiate between the extended ICM emission and a cooling flow component. The sum of the two is encapsulated in the L-M relation. The log N–log S relation shown in Figure 3 exhibits two extremes. The bold lines show the expectations assuming that the bulk of the cluster emission follows the extended β-profile form of equation (9), while the light lines are calculated assuming all of the cluster emission is captured by the detect cell. This latter case could be interpreted as an extreme case of a central cooling flow emitting all of the cluster X-rays with no extended emission. From Figure 3, the counts using all the flux run about a factor 2–3 higher than those expected assuming extended emission. The hybrid assumption considered by Pesce et al. is likely to be intermediate between these two cases.

Analysis of *EXOSAT* data by Edge & Stewart 1991 indicates that a typical contribution of cooling flows is $\sim 20\%$ of the total luminosity. Referring to Figure 2, the 4.8 arcmin^2 detect cell we employ would capture roughly 40% of the flux from a 300 kpc core radius cluster at a redshift of 0.2, the median redshift expected for the NEP sample. At this redshift, the core radius has an angular size of about 1′. Adding an additional 20% as a typical cooling flow contribution would increase the detect cell flux by $\sim 40\%$, not a significant amount. For clusters with larger angular core radii, the effect can be more significant. The cooling flow contribution would double the detect cell flux for a cluster with an angular core radius of 3′. The larger effect seen by Pesce et al. can be attrib-

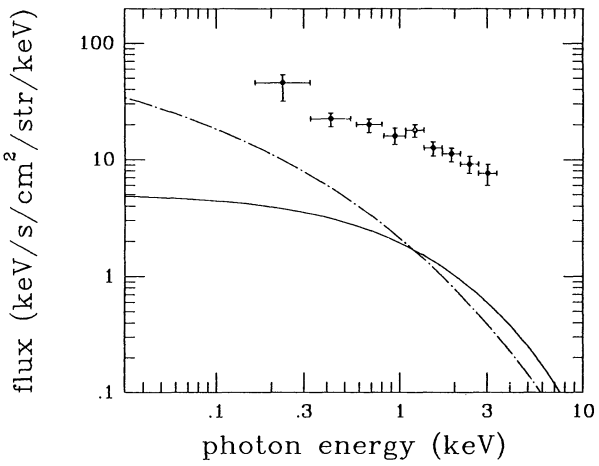

FIG. 6.—The spectrum of the X-ray background contributed by cluster sources. The observational data shown are taken from Wu et al. (1990). Model XCDM (*dot-dashed line*) predicts a softer spectrum than model CDMP3 (*solid line*).

uted to a combination of the smaller detect cell and the poorer resolution of the *Einstein* IPC. For example, we find a factor 20 difference in predicted counts between the full flux and extended cases for a 2'.4 detect cell and Gaussian smearing on a scale of 1'.5.

4.3. *Uncertainties in Empirical Normalization*

Another possible source of systematic error in the number count predictions comes from uncertainty in the amplitude of the local luminosity function. Our models are normalized to the EMSS data of Gioia et al. (1990a). Their fit to a power-law form for the luminosity function $N(L)dL = AL^{-\alpha}dL$ with L in units of 10^{44} ergs s^{-1} produces a slope of $\alpha = 2.1 \pm 0.2$ and an amplitude of $A_{\rm EMSS} = 7.2 \pm 0.6$ Mpc^{-3} in the nearest redshift bin. The *EXOSAT* data of Edge et al. (1990), covering a similar luminosity and redshift range, are fitted well by a power law of similar slope, but much lower amplitude $A_{\rm EXOSAT} = 2.2 \times 10^{\pm 0.11}$ Mpc^{-3}. Band corrections may provide at least a partial remedy. However, for the fiducial cluster ICM temperature of 7 keV assumed by Gioia et al., equal fractions of the bolometric luminosity emerge in the 0.3–3.5 keV and 2–10 keV ranges. At lower cluster temperatures, more flux emerges in the *Einstein* band than the *EXOSAT*. This goes in the right direction to reconcile the two normalizations. It is beyond the scope of this paper to attempt a full resolution of this issue. We draw attention to it in order to caution the reader that systematic uncertainties at the factor 2 level exist in present, low-z luminosity function determinations. We expect data from *ROSAT* will provide an improved normalization.

5. SUMMARY

We have presented theoretical models for the evolution of X-ray cluster abundances, with the principal aim of establishing predictions for the cluster population to be seen in the *ROSAT* survey. The most natural model, which assumes a self-similar population in a CDM universe, is ruled out by the shape of the local luminosity function. This result was already evident in the analysis of Gioia et al. (1990a), and a similar conclusion has been reached in a model-independent fashion by Kaiser (1991). Two alternative models—one working within CDM with an $L \propto M^3$ luminosity-mass relation, the other employing an $n = -2$ spectrum with $L \propto M^{11/6}$—both provided good fits to the local cluster abundance data. The scalings in the former model can arise if the ICM fraction scales nearly proportionally to the cluster binding mass while those in the latter model can result if the entropy of the gas in cluster cores is fixed, perhaps via feedback during the galaxy or quasar formation era.

With a square detect cell of side 4'.8 employed to search for extended cluster sources, we expect roughly 200 clusters per steradian above the all-sky survey limiting flux of 7×10^{-13} ergs s^{-1} cm^{-2}. For the north ecliptic pole region of the *ROSAT* survey, which will cover a 10° radius field to a limiting flux of roughly 9×10^{-14} ergs s^{-1} cm^{-2}, both successful models predict $\sim$330 cluster X-ray sources. The clusters would have a median redshift of 0.2 and 10% of them should have $z > 0.4$. We expect there to be essentially no chance of finding clusters at redshifts greater than one in the NEP.

The two successful models which predict identical counts are potentially distinguishable by the number of clusters as a function of temperature (or, equivalently, the T-L relation) as well as the contribution of clusters to the extragalactic X-ray background at very soft energies $\sim$0.1 keV. Such independent observational data are required to break the redundancy between cosmological and evolutionary factors influencing count predictions. At 1 keV, both models predict roughly 10% of the observed X-ray background arises from clusters.

Finally, we would not at all be dissatisfied if the *ROSAT* data fail to conform to the predictions of these relatively simple models but, instead, provide evidence for new and exciting phenomena to challenge theorists and observers in coming years.

We thank N. Kaiser, A. Fabian, A. Edge, & G. Hasinger for useful input. J. P. H. would like to thank Professor Truemper and the *ROSAT* group for hospitality and acknowledges support from NASA *ROSAT* grant NAG5-1256 and NSF grant INT 8912660. A. E. E. was supported in part by the Miller Foundation for Basic Research in Science at the University of California, Berkeley and by NASA Theory grant 10-56388.

APPENDIX A

ABUNDANCE FUNCTION FOR POWER-LAW FORMS

We would like to calculate the number density of objects as a function of some observable Y (luminosity, temperature, etc.) which scales with binding mass and redshift as

$$Y = Y_{15} M^p (1+z)^s , \tag{A1}$$

where the mass M is in $10^{15}\ M_\odot$ and Y_{15} is the present normalization at that mass scale. Solving for M in the above expression allows equation (3) of § 2 to be transformed

$$n(Y, z)dY = \hat{n}_*(z) Y^{-(p+1-\alpha)/p} \exp\left[-(Y/Y_*(z)]^{2\alpha/p}\right) dY , \tag{A2}$$

where

$$\begin{aligned} Y_*(z) &= (1.19/\sigma_{15})^{-p/\alpha}(1+z)^{s-p/\alpha} Y_{15} , \\ \hat{n}_*(z) &= 9.3 \times 10^{-5} (\alpha Y_{15}/\sigma_{15}^p)(1+z)^{1+s(1-\alpha)/p}\ \text{Mpc}^{-3} . \end{aligned} \tag{A3}$$

APPENDIX B

SCALING LAWS FOR MINIMUM CENTRAL ENTROPY

Let us begin with a spherically symmetric cluster with gas temperature $T(r)$ and density profile $\rho(r)$, for which the bolometric X-ray luminosity from bremsstrahlung scales as

$$L_{\rm bol} \propto \int dr\, r^2 \rho^2(r) T^{1/2}(r) \,. \tag{B1}$$

Assume the temperature profile is isothermal $T(r)$ = constant and that the virial theorem applies so that the temperature scales with cluster binding mass and redshift as $T \sim M^{2/3}(1+z)$. Further, we write the density profile in the usual form

$$\rho(r) = \rho_c [1 + (r/r_c)^2]^{-3\beta/2} \,, \tag{B2}$$

where the core radius r_c and central density ρ_c also depend on M and z. Consider the virial radius r_v, defined as the radius within which the mean density is ~ 170 times the background value $\rho_b(z)$. If the baryonic ICM mass systematically traces the binding mass within r_v (numerical experiments of Evrard 1990a show this to hold to within $\sim 15\%$), then the following relation between core and virial properties holds:

$$\left(\frac{r_c}{r_v}\right)^3 \sim \left[\frac{\rho_c}{\rho_b(z)}\right]^{-1/\beta} \,. \tag{B3}$$

The bolometric luminosity emitted by the relaxed portion of the cluster

$$L_{\rm bol} \propto T^{1/2} \rho_c^2 \int_0^{r_v} dr\, r^2 [1 + (r/r_c)^2]^{-3\beta} \tag{B4}$$

is then found to scale as

$$L_{\rm bol} \propto T^{1/2} \rho_c^2 (r_c/r_v)^3 [M/\rho_b(z)] \int_0^{r_v/r_c} dy\, y^2 (1+y)^{-3\beta} \,. \tag{B5}$$

For a fixed value of β, the integral above is a constant, then using equation (B3) and the fact that $\rho_b(z) \propto (1+z)^3$ gives

$$L_{\rm bol} \propto T^{1/2} \rho_c^{2-1/\beta} M (1+z)^{3(1/\beta - 1)} \,. \tag{B6}$$

Assume that some "agent" (feedback from galaxy or quasar formation?) preheats the "proto–intracluster medium" to some characteristic temperature T_i at some early epoch z_i, thereby establishing a characteristic entropy $s_i = \ln(T_i/\rho(z_i)^{\gamma-1})$. As collapse proceeds, the central cluster gas may remain adiabatic while outer layers are subsequently shocked to higher entropies. The resultant, postcollapse temperature profile is likely to be close to the isothermal assumption used in writing equation (B4) (Evrard 1990a). However, in this scenario, the gas in the cores of rich clusters remembers its initial adiabat, implying the core density will scale with cluster temperature as $\rho_c \propto T^{1/(\gamma-1)}$. For $\gamma = 5/3$, this yields

$$\rho_c \propto T^{3/2} \propto M (1+z)^{3/2} \,. \tag{B7}$$

Applying this to equation (B6) with $\beta = 2/3$ produces the scalings used for model XCDM

$$L_{\rm bol} \propto M^{11/6} (1+z)^{11/4} \,. \tag{B8}$$

The scaling of the core radius with mass and redshift follows from equations (B3) and (B7)

$$r_c \propto M^{-1/6} (1+z)^{-1/4} \,. \tag{B9}$$

REFERENCES

Abramopolous, F., & Ku, W. 1983, ApJ, 271, 446
Blanchard, A., Wachter, K., Evrard, A. E., & Silk, J. 1992, ApJ, in press
Blumenthal, G. R., Faber, S. M., Primack, J. R., & Rees, M. J. 1984, Nature, 311, 517
Bond, J. R., Cole, S., Efstathiou, G., & Kaiser, N. 1991, preprint
Broadhurst, T. J., Ellis, R. S., Koo, D. C., & Szalay, A. S. 1990, Nature, 343, 726
Cole, S. 1991, ApJ, 367, 45
Cruddace, R. G., Hasinger, G., & Hartner, G. 1991, Exper. Astr., in press
David, L. P., Arnaud, K. A., Forman, W., & Jones, C. 1990, ApJ, 356, 32
Davis, M., Efstathiou, G., Frenk, C. S., & White, S. D. M. 1985, ApJ, 292, 371
Edge, A. C., & Stewart, G. C. 1991, MNRAS, submitted
Edge, A., Stewart, G. C., Fabian, A. C., & Arnaud, K. A. 1990, MNRAS, 245, 559
Efstathiou, G., Frenk, C. S., White, S. D. M., & Davis, M. 1988, MNRAS, 234, 715
Efstathiou, G., Kaiser, N., Saunders, W., Lawrence, A., Rowan-Robinson, M., Ellis, R. S., & Frenk, C. S. 1990, MNRAS, 247, 10P
Evrard, A. E. 1989, ApJ, 341, 26
———. 1990a, ApJ, 363, 349
———. 1990b, in Clusters of Galaxies, ed. W. R. Oegerle, M. J. Fitchett, & L. Danly (Cambridge: Cambridge Univ. Press), 287
Fabian, A. C., Nulsen, P. E. J., & Canizares, C. R. 1984, Nature, 310, 733
Gioia, I. M., Henry, J. P., Maccacaro, T., Morris, S. L., Stocke, J. T., & Wolter, A. 1990a, ApJ, 356, L35
Gioia, I. M., Maccacaro, T., Schild, R. E., Wolter, A., Stocke, J. T., Morris, S. L., & Henry, J. P. 1990b, ApJS, 72, 567
Hasinger, G. 1985, Bull. d'Information du Centre de Données Stellaires, 28, 87
Henry, J. P., & Arnaud, K. A. 1991, ApJ, 372, 410
Hughes, J. P. 1989, ApJ, 337, 21
Johnson, M. W., Cruddace, R. G., Ulmer, M. P., Kowalski, M. P., & Wood, K. S. 1983, ApJ, 266, 425
Kaiser, N. 1986, MNRAS, 222, 323
———. 1991, ApJ, 383, 104
Lahav, O., Edge, A., Fabian, A. C., & Putney, A. 1989, MNRAS, 238, 881
Maddox, S. J., Efstathiou, G., Sutherland, W. J., & Loveday, J. 1990, MNRAS, 242, 43P
McCammon, D., Burrows, D. N., Sanders, W. T., & Kraushaar, W. L. 1983, ApJ, 269, 107
McCammon, D., & Sanders, W. T. 1990, ARA&A, 28, 657
McKee, J. D., Mushotsky, R. F., Boldt, E. A., Holt, S. S., Marshall, F. E., Pravdo, S. H., & Serlemitsos, P. J. 1980, ApJ, 242, 843
Peebles, P. J. E. 1980, The Large-Scale Structure of the Universe (Princeton: Princeton Univ. Press)
———. 1982, ApJ, 257, 438

Perrenod, S. C. 1980, ApJ, 236, 373
Pesce, J. E., Fabian, A. C., Edge, A. C., & Johnstone, R. M. 1990, MNRAS, 244, 58
Piccinotti, G., Mushotzky, R. F., Boldt, E. A., Holt, S. S., Marshall, F. E., Serlemitsos, P, J., & Shafer, R. A. 1982, ApJ, 253, 485
Press, W. H., & Schechter, P. 1974, ApJ, 187, 425
Rothenflug, R., & Arnaud, K. A. 1985, A&A, 144, 431
Sarazin, C. L. 1986, Rev. Mod. Phys., 58, 1
Truemper, J. 1984, Phys. Scripta, T7, 209
White, R. E. 1990, ApJ, 367, 69
White, S. D. M., & Frenk, C. S. 1991, ApJ, 379, 52
Wu, X., Hamilton, T., Helfand, D. J., & Wang, Q. 1991, ApJ, 379, 564